optica

Field-resolved detection of the temporal response of a single plasmonic antenna in the mid-infrared

Marco P. Fischer,[1] Nicolò Maccaferri,[2] Kevin Gallacher,[3] Jacopo Frigerio,[4] Giovanni Pellegrini,[5] Douglas J. Paul,[3] Giovanni Isella,[4] Alfred Leitenstorfer,[1] Paolo Biagioni,[6] and Daniele Brida[1,2,*]

[1]Department of Physics and Center for Applied Photonics, University of Konstanz, D-78457 Konstanz, Germany
[2]Department of Physics and Materials Science, University of Luxembourg, 162a, avenue de la Faïencerie L-1511, Luxembourg, Luxembourg
[3]School of Engineering, University of Glasgow, Rankine Building, Oakfield Avenue, Glasgow, G12 8LT, UK
[4]L-NESS, Dipartimento di Fisica del Politecnico di Milano, Via Anzani 42, 22100 Como, Italy
[5]Dipartimento di Fisica, Università di Pavia, Via Agostino Bassi 6, 27100 Pavia, Italy
[6]Dipartimento di Fisica, Politecnico di Milano, Piazza Leonardo da Vinci 32, 20133 Milano, Italy
*Corresponding author: daniele.brida@uni.lu

Received 25 January 2021; revised 9 April 2021; accepted 10 April 2021 (Doc. ID 420683); published 14 June 2021

Unveiling the spatial and temporal dynamics of a light pulse interacting with nanosized objects is of extreme importance to widen our understanding of how photons interact with matter at the nanoscale and trigger physical and photochemical phenomena. An ideal platform to study light–matter interactions with an unprecedented spatial resolution is represented by plasmonics, which enables an extreme confinement of optical energy into sub-wavelength volumes. The ability to resolve and control the dynamics of this energy confinement on the time scale of a single optical cycle is at the ultimate frontier towards a full control of nanoscale phenomena. Here, we resolve in the time domain the linear behavior of a single germanium plasmonic antenna in the mid-infrared by measuring the complex optical field response in amplitude and phase with sub-optical-cycle precision, with the promise to extend the observation of light–matter interactions in the time domain to single quantum objects. Accessing this fundamental information opens a plethora of opportunities in a variety of research areas based on plasmon-mediated photonic processes and their coherent control, such as plasmon-enhanced chemical reactions and energy harvesting.

https://doi.org/10.1364/OPTICA.420683

1. INTRODUCTION

A full understanding of light–matter interactions at the nanoscale can be enabled by resolving and correlating both the spatial and temporal structure of a light pulse interacting with nanoscale materials and molecules. From a spatial point of view, we have already reached a wide understanding of many nanoscale light–matter coupling phenomena in their ground state. On the contrary, unveiling the temporal evolution related to excited states or to coherent dynamics of many light–matter interactions is still quite challenging. Furthermore, the manipulation of highly intense and ultrashort light pulses plays a crucial role in energy harvesting and chemical reactions and, in general, will impact on new technologies exploiting ultrafast phenomena in condensed matter. In recent years plasmonics [1,2], and especially plasmonic nanoantennas [3–7], has received broad attention in nanophotonics, opening up valuable opportunities to enhance light–matter interactions for sensing [8–11], energy harvesting [12,13], and opto-electronics [14–16]. Moreover, owing to the large field enhancement over sub-diffraction limited volumes, various applications ranging from near-field microscopy [17,18] to ultra-sensitive material detection [19,20] and to the observation of higher-order optical nonlinearities [21–24] are heavily investigated. First studies were performed in the visible and near-infrared spectral range, generally based on noble-metal subwavelength structures. These investigations enabled an unprecedented understanding, along with the active manipulation, of many physical phenomena occurring at the nanoscale and usually hidden below the noise level of standard experimental techniques.

With the exploitation of heavily doped semiconductors as a new class of plasmonic materials [25–31], the research expanded into the mid-infrared spectral region, which is an extremely appealing frequency range because it coincides with the fingerprint region of many molecular vibrations. Plasmonic antennas in this range can then help, for instance, to resolve in amplitude and phase specific molecular dynamics in both the frequency and time domains. While classic intensity [7] or polarization [32,33] detection schemes allow one to study the resonance behavior in its steady state, the underlying temporal dynamics, as well as the extremely fast (few fs) response of a resonant antenna remain hidden. Nonlinear femtosecond spectroscopy [21,34–38] in combination with electromagnetic simulations [36,39,40] can be employed to gain insight into these dynamics and to extract the

temporal information that underlies both linear and nonlinear processes. In particular, knowledge of the exact field evolution with sub-optical-cycle precision allows one to observe coherent dephasing mechanisms, an aspect that is crucial for the understanding of nonlinear effects in nanostructures coupled to molecular systems supporting a plethora of resonant modes (e.g., plasmons, photons, or excitons). Current approaches, although very powerful, require a complex implementation and none of the standard methodologies based on linear detection schemes allows for a complete resolution of the optical field in both amplitude and phase. In the visible and near-infrared spectral ranges, this information is very difficult to retrieve since the carrier frequency is too high to allow a direct observation of sub-optical-cycle dynamics on a single and isolated nanostructure. In fact, attosecond spectroscopy is in its infancy, and the sensitivity necessary for this kind of measurement is still out of reach. There have been many efforts to use nonlinear optics and electron emission to fit the temporal near-field electromagnetic response of nanostructures in this spectral range, although not providing a direct measurement of the amplitude and phase of the optical field [34,41–44]. In the mid-infrared spectral range, however, the full characterization in amplitude and phase of optical pulses becomes possible at the high level of sensitivity required to observe the complex response of an isolated antenna, with a huge potential to expand our knowledge of light–matter interactions in the THz spectral range, beyond what is offered by the classical pump–probe techniques accessing only the charge dynamics. First attempts in this direction have been proposed by several groups, although they were limited to the sub-THz spectral region [45–51]. Here, we demonstrate that the oscillating optical field $\mathbf{E_0}$ of a light pulse interacting with a single plasmonic antenna and shaped by its resonance can be measured by femtosecond multi-THz (or mid-infrared) time-domain spectroscopy (TDS) [52–54] combined with high-resolution confocal microscopy. Our experiments promise to extend the observation of field-resolved light–matter interaction in the time domain to single quantum objects in the proximity of plasmonic nanostructures at higher energies, that is at tens of THz.

2. RESULTS

Sensitive electro-optic sampling TDS (EOS-TDS) is employed for the detection of transmitted fields in a confocal transmission geometry with a high numerical aperture (see Fig. 1 and a detailed description in the Methods section). All the double-rod antennas are fabricated from heavily doped germanium (see Methods) and feature arms with a thickness of 1.4 μm and a width of 1.0 μm and a gap width of 300 nm, while the arm length and thus the aspect ratio and resonance frequency are varied within the sample.

Figure 2(a) shows the experimental transient real part of the impinging electric field. We plot both the electric field of the probe pulse after propagation through the bare silicon substrate ($Re[E_{0x}]$, blue graph) and the electric field of the probe pulse interacting with both substrate and a Ge double-rod antenna of arm length 5.5 μm in the microscope focal area ($Re[E_x]$, red graph). The two curves are normalized to the maximum value of $Re[E_{0x}]$. A linear subtraction between $Re[E_{0x}]$ [Fig. 2(a), blue graph] and $Re[E_x]$ [Fig. 2(a), red graph] provides a time-resolved differential signature of the interaction between the optical waveform and the antenna [Fig. 2(b), green graph].

With this approach, we can follow the non-trivial response of the plasmonic antenna represented by a clear phase jump of the oscillation occurring at approximately 50 fs [Figs. 2(b) and 2(d), dashed orange line]. Three-dimensional finite-difference time-domain (FDTD) simulations were also performed to extract the femtosecond sub-cycle dynamics, as reported in Figs. 2(c) and 2(d), for the representative case of the Ge antenna with an arm length of 5.5 μm (see Methods for more details). In particular, Fig. 2(d) confirms how the antenna response moves from out-of-phase to

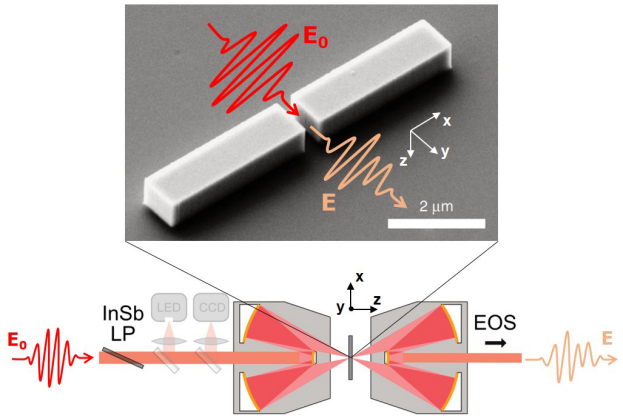

Fig. 1. Scanning electron microscope image of a single double-rod antenna structure with an arm length of 3.5 μm fabricated from heavily doped germanium on a silicon substrate. The red transient represents the incoming incident pulse field E_0, while the pink one is the pulse after the interaction with the Ge antenna. The light propagates along the z direction, while the beam is polarized along the x direction parallel to the long axis of the antenna. The bottom panel shows a sketch of the experimental setup used for the electro-optical sampling time-domain spectroscopy (EOS-TDS) of the transient signal after interaction with the antenna. LP, low pass filter; LED, white light emitting diode; CCD, charge-coupled device. LED and CCD are used to align the microscope.

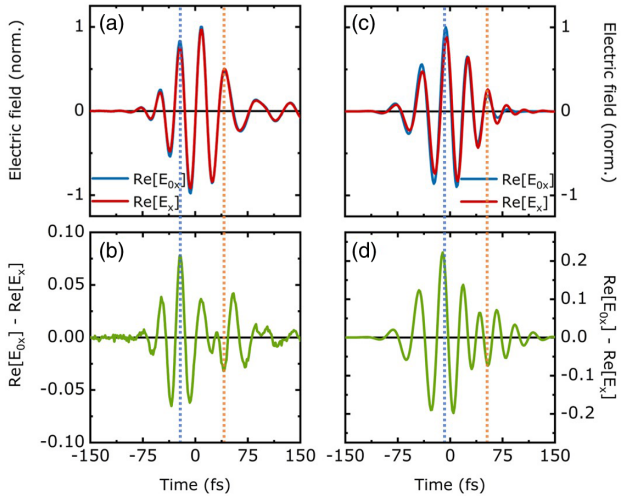

Fig. 2. Multi-THz TDS on a heavily doped Ge antenna with arm lengths of 5.5 μm: (a) $Re[E_x]$ after interaction with the antenna (red), in comparison to the probe pulse $Re[E_{0x}]$ not interacting with the antenna (blue), normalized to maximum of $Re[E_{0x}]$; (b) TDS antenna response field amplitude by subtraction of the curves plotted in (a); (c) FDTD calculated $Re[E_{0x}]$ $|E_0|$ (blue) and $Re[E_x]$ (red) normalized to the maximum of $Re[E_{0x}]$; (d) calculated antenna response field amplitude by subtraction of the curves plotted in (c). The colored dashed lines are eye-guides to highlight the in-phase (blue) and phase jump (orange) cases.

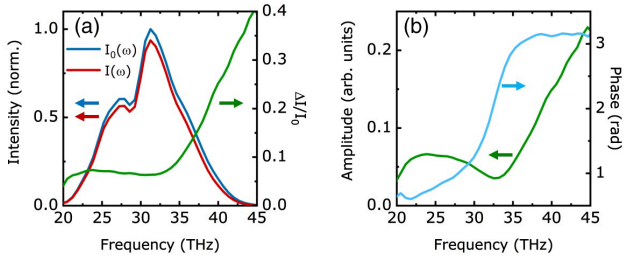

Fig. 3. (a) Experimental intensity spectra with and without antenna interaction obtained via fast Fourier transform (FFT; red and blue, respectively) normalized to the intensity I_0 of the unperturbed incident electric field, and experimental differential transmission $\Delta I/I_0$ (green); (b) spectral response function in amplitude (green) and phase (blue) of a single antenna obtained via FFT of the temporal response difference signal plotted in Fig. 2(b).

in-phase within the few optical cycle excitation, in good agreement with the experimental results in Figs. 2(a) and 2(b).

By evaluating the fast Fourier transform (FFT) of the signals in Fig. 2(a), we obtain the frequency-dependent response of the background (substrate) $I_0 = |\mathbf{E_0}|^2$, and of the antenna on the substrate $I = |\mathbf{E}|^2$ [Fig. 3(a), blue line and red line, respectively, both normalized to the maximum of I_0]. By subtracting the two curves and normalizing them to the background signal I_0, we extract the differential transmission of the single antenna $\Delta I/I_0 = (I_0 - I)/I_0$, which displays a clear dip around 32.5 THz, indicating the presence of a resonant mode. If we now perform the FFT of the signal in Fig. 2(b), we obtain the response of the antenna in amplitude and phase in the frequency domain [Fig. 3(b), green and blue curves, respectively]. Noticeably, the matching between the differential transmission and the field amplitude dips confirms that the antenna response is due to the excitation of a resonant mode at 32.5 THz.

For completeness and for testing the robustness of our approach, we performed the same experiment on antennas where we varied the arm length to tune the plasmonic resonance position, and extracted the spectral response of all the antennas in the frequency domain [Fig. 4(a)]. Furthermore, FDTD simulations were performed to reproduce the observed differential transmission spectra (see also Supplement 1, Fig. S1 for the absorption spectra and near-field profiles). The calculations reproduce well the spectral dependence of the differential transmission as a function of the wavelength [Fig. 4(b)]. By increasing the arm length, a redshift of the main spectral features is observed. The slight disagreement between the measured and experimental curves is due to the complexity of a 3D problem with a strongly focused Gaussian, which is difficult to tackle numerically. In more detail, although in the simulation we considered as approximation an impinging Gaussian beam, in the experiment, we use Cassegrain objectives to focus the beam. Thus, the beam impinging on the structures deviates from a perfect Gaussian. Moreover, some wave vectors are not contributing to the excitation of light emission from the antenna due to the hollowness of both the illumination and the collection beams. Another cause of discrepancy can be that in the experiment, the beam might not be focused on the same plane as it is in the simulation, thus having a slightly different field distribution because of the field gradients in the focal volume. Finally, also the Gouy phase shift, when combined with the actual placement of the antenna with respect to the ideal focal plane, might contribute to the small discrepancy between measured and calculated curves. The small redshift of the experimental response compared to the calculated one, can be also inferred to the aforementioned reasons.

It is worth mentioning here that, with our approach, it is clearly possible to experimentally access both the complex frequency- and time-resolved response of a single plasmonic antenna at tens of THz, until now possible only by using theoretical approaches such as the FDTD method. Moreover, by knowledge of either the spectral response at a certain time delay or of the temporal response at a specific frequency, we can reconstruct the transient response as a function of both time and frequency via the Wigner distribution function (WDF) [55], which allows us to describe the nanostructure response during the interaction with an external light pulse. Thus, we can estimate the frequency–time distribution of the antenna response, since we can directly measure the field response in the time domain. In our case, the temporal profile of the incident light pulse interacting with the substrate only or with the antenna with an arm length of 5.5 μm has been measured [Figs. 2(a), blue and red curve, respectively]. By subtracting the two signals and correcting for the offset phase of the background probe signal introduced by the measurement, we finally obtained the WDF for the response of the antenna [Fig. 5(a)]. As inferred by the color map, the response of the antenna shows a secondary peak at positive delays centered at 32.5 THz. This effect represents a time–frequency manifestation of the phase jump that occurs in an oscillator between frequencies above and below resonance [Figs. 2(b) and 2(d), orange line]. The overall response is additionally enriched by interference effects, possibly due to the finite thickness of the antenna, that determine an increase of the extinction at approximately 40 THz. These effects are observable by the modulation of the frequency response at 38 THz that occurs approximately at a delay of 25 fs. We have also calculated the WDF from the data plotted in Fig. 2(c), and the result is presented in Fig. 5(b). As can be seen, the main features of the time–frequency response of the antenna are well reproduced. It is worth mentioning here that although the matching between the calculated WDF and the experimental one is remarkable, there are also small discrepancies between experiment and calculation. This means that even if numerically one can predict well the antenna response, it is very important to experimentally access the full-field response of the real system, in particular in view of applications where other

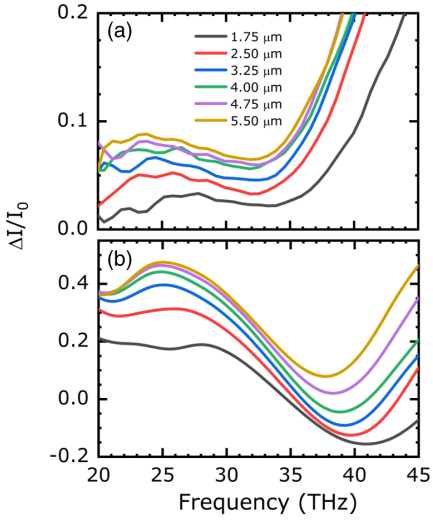

Fig. 4. (a) Experimental differential transmissions of single antennas for various arm lengths. (b) FDTD simulated differential transmissions in the frequency domain.

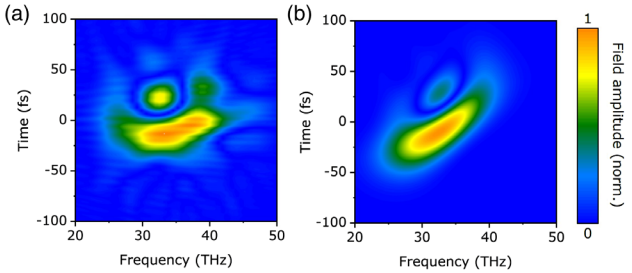

Fig. 5. (a) WDF of the experimental normalized electric field amplitude of a Ge antenna with an arm length of 5.5 μm. (b) WDF of the simulated normalized electric field amplitude of a Ge antenna with an arm length of 5.5 μm.

objects, e.g., molecules or quantum emitters, are coupled with the antenna, and discrepancies with the numerical calculations might play a pivotal role in eventual coupling mechanisms.

3. CONCLUSIONS

In conclusion, we have demonstrated that with EOS-TDS it is possible to acquire experimentally the complete response of the linear interaction between a light pulse and a single semiconductor plasmonic antenna resonant in the mid-infrared by resolving the time-dependent optical field with a sub-cycle temporal resolution. We have shown that the direct extraction of the complex spectral response (in amplitude and phase) of a single antenna is possible beyond the current state of the art in EOS-TDS. Since we can observe the resonance in amplitude and phase, we can tailor an optical waveform to drive the plasmonic oscillation by enhancing it or switching it off completely by a suitable interference between plasmons and external fields. While the mid-infrared spectral window is especially appealing because it contains the fingerprint of vibrational resonances of complex molecules, we foresee that this approach might be pushed to resolve the full response of nanostructures also in the near-infrared and visible ranges, owing to emerging attosecond technologies [56] and to coherent control of localized plasmons by tailored waveforms. Moreover, this method can be applied to enhance light–matter interactions with the plasmonic resonance and shine new light on unexplored molecular dynamics in the mid-infrared by experimentally accessing the effect of the plasmon-enhanced electric field on coherent dynamics and the manipulation of photochemical reactions, for instance, by using one-shot EOS-TDS schemes [57,58]. Additionally, new degrees of freedom will be enabled by the engineering of antenna structures with the possibility to shape the field response of the antenna. This perspective is particularly appealing since it will be possible to shape the optical field in the proximity of the antennas with the aim to control the coherent dynamics of individual molecules or quantized nanosystems.

4. METHODS

Fabrication. Heavily doped germanium antenna structures with resonance in the mid-infrared were fabricated via electron beam lithography and reactive ion etching from epitaxial films on a silicon substrate [20,31,59]. By means of low-energy plasma-enhanced chemical vapor deposition, high-quality single crystalline growth with *in situ* phosphorous doping was performed, with an activated donator concentration of about 2.5×10^{19} cm^{-3} [30].

Optical setup and antenna characterization. Isolated double-rod antenna structures with varying arm lengths were measured in a confocal microscopy setup based on two Cassegrain-geometry all-reflective objectives (36×, NA = 0.5). To probe the antenna response, broadband phase-stable femtosecond pulses in the mid-infrared/multi-THz frequency range were generated via phase-matched difference frequency generation in GaSe bulk crystals [60]. At a bandwidth of 10.7 THz, the pulse duration equals 58 fs. The maximum peak field is 5 MV/cm, but the peak amplitude is attenuated to be lower than 100 kV/cm in the experiments. An Yb:KGW high-power laser system (*Light Conversion, Pharos 10 W*) with a repetition rate of 50 kHz was used to guarantee large acquisition rates to reduce statistical noise [61]. The antenna response was detected in transmission geometry via sensitive EOS-TDS in thin GaSe crystals (thickness 80 μm) [60]. As EOS-TDS gating pulses, a broadband white light supercontinuum was generated in a bulk YAG crystal and compressed to sub-15 fs durations [61,62]. To avoid phase fluctuations within the acquisition time, transients were recorded in fast-scan mode at an acquisition rate of 5 Hz using a piezo delay scanner. Low-noise detection was accomplished by employing a boxcar amplifier (*Zurich Instruments, UHF-BOX*) on a shot-to-shot basis in combination with an optimized ellipsometry balanced detection scheme (*Thorlabs, PDB440C*). The presented data were averaged from 1250 recorded transients each. A cross correlation algorithm was employed to compensate for the timing jitter between single measurements before averaging was undertaken.

FDTD simulations. Electromagnetic simulations for the linear optical response of Ge antennas were performed with the FDTD method using a commercial software [63]. The frequency-dependent dielectric constant of heavily doped Ge was characterized experimentally by Fourier-transform infrared spectroscopy [30] (see also Supplement 1, Fig. S2), while for Si, we adopt a constant real-valued refractive index of $n = 3.4$. High-accuracy conformal meshing was used for the air and substrate discretization, while a finer cell size of 30 nm was forced in the region of the antenna. For all the simulations, a Gaussian illumination resembling the experimental numerical aperture (0.5) was employed. The convergence criterion was set to halt the simulations once the electromagnetic energy initially injected into the simulation volume by the source was reduced by a factor 10^{-5}. The time-domain evolution of the electric field was recorded with a point field monitor located 5 μm below the sample surface, i.e., inside the Si substrate. This monitor provides directly the time evolution of the complex (amplitude and phase) electric field, as plotted in Fig. 2(c). The same quantity is then processed with the same procedure as for the experimental data to obtain the map in Fig. 5(b). Intensity spectra were obtained by collecting spatially resolved field spectra (amplitude and phase), as obtained by Fourier-transforming the respective time evolutions, over an ideally infinite plane located 5 nm below the antenna–substrate interface. A numerical far-field projection of such near fields is then performed with the software built-in function to obtain the intensity distribution over a sphere of 1 m radius centered on the antenna position, which is then integrated over the angular acceptance of the collection objective. Finally, absorption spectra were extracted from the net flux of the Poynting vector entering the antenna volume, as measured by a closed box monitor surrounding the whole antenna.

Funding. European Regional Development Fund (2017-03-022-19); Fonds National de la Recherche Luxembourg (C19/MS/13624497); European Research Council (819871); European Commission (613055).

Disclosures. The authors declare no conflicts of interest.

Data Availability. Data underlying the results presented in this paper are not publicly available at this time but may be obtained from the authors upon reasonable request.

Supplemental document. See Supplement 1 for supporting content.

REFERENCES

1. H. A. Atwater, "The promise of plasmonics," Sci. Am. **296**, 56 (2007).
2. S. A. Maier, *Plasmonics—Fundamentals and Applications* (Springer, 2007).
3. K. B. Crozier, A. Sundaramurthy, G. S. Kino, and C. F. Quate, "Optical antennas: resonators for local field enhancement," J. Appl. Phys. **94**, 4632 (2003).
4. P. Mühlschlegel, H.-J. Eisler, O. J. F. Martin, B. Hecht, and D. W. Pohl, "Resonant optical antennas," Science **308**, 1607 (2005).
5. P. Bharadwaj, B. Deutsch, and L. Novotny, "Optical antennas," Adv. Opt. Photon. **1**, 438–483 (2009).
6. L. Novotny and N. van Hulst, "Antennas for light," Nat. Photonics **5**, 83–90 (2011).
7. P. Biagioni, J.-S. Huang, and B. Hecht, "Nanoantennas for visible and infrared radiation," Rep. Prog. Phys. **75**, 24402 (2012).
8. F. Neubrech, A. Pucci, T. W. Cornelius, S. Karim, A. García-Etxarri, and J. J. Aizpurua, "Resonant plasmonic and vibrational coupling in a tailored nanoantenna for infrared detection," Phys. Rev. Lett. **101**, 157403 (2008).
9. R. Adato, A. A. Yanik, J. J. Amsden, D. L. Kaplan, F. G. Omenetto, M. K. Hong, S. Erramilli, and H. Altug, "Ultra-sensitive vibrational spectroscopy of protein monolayers with plasmonic nanoantenna arrays," Proc. Natl. Acad. Sci. USA **106**, 19227 (2009).
10. L. V. Brown, K. Zhao, V. King, H. Sobhani, P. Nordlander, and N. J. Halas, "Surface-enhanced infrared absorption using individual cross antennas tailored to chemical moieties," J. Am. Chem. Soc. **135**, 3688 (2013).
11. C. Huck, J. Vogt, M. Sendner, D. Hengstler, F. Neubrech, and A. Pucci, "Plasmonic enhancement of infrared vibrational signals: nanoslits versus nanorods," ACS Photon. **2**, 1489–1497 (2015).
12. H. A. Atwater and A. Polman, "Plasmonics for improved photovoltaic devices," Nat. Mater. **9**, 205–213 (2010).
13. S. Carretero-Palacios, A. Jiménez-Solano, and H. Míguez, "Plasmonic nanoparticles as light-harvesting enhancers in perovskite solar cells: a user's guide," ACS Energy Lett. **1**, 323–331 (2016).
14. B. Schwarz, P. Reininger, D. Ristanic, H. Detz, A. M. Andrews, W. Schrenk, and G. Strasser, "Monolithically integrated mid-infrared lab-on-a-chip using plasmonics and quantum cascade structures," Nat. Commun. **5**, 4085 (2014).
15. L. Zhang, A. M. Agarwal, L. C. Kimerling, and J. Michel, "Nonlinear group IV photonics based on silicon and germanium: from near-infrared to mid-infrared," Nanophotonics **3**, 247–268 (2014).
16. T. J. Davis, D. E. Gómez, and A. Roberts, "Plasmonic circuits for manipulating optical information," Nanophotonics **6**, 543–559 (2017).
17. S. Palomba and L. Novotny, "Near-field imaging with a localized nonlinear light source," Nano Lett. **9**, 3801–3804 (2009).
18. E. Sakat, V. Giliberti, M. Bollani, A. Notargiacomo, M. Pea, M. Finazzi, G. Pellegrini, J.-P. Hugonin, A. Weber-Bargioni, M. Melli, S. Sassolini, S. Cabrini, P. Biagioni, M. Ortolani, and L. Baldassarre, "Near-field imaging of free carriers in ZnO nanowires with a scanning probe tip made of heavily doped germanium," Phys. Rev. Appl. **8**, 54042 (2017).
19. E.-P. Li and H.-S. Chu, *Plasmonic Nanoelectronics and Sensing* (Cambridge, 2014).
20. L. Baldassarre, E. Sakat, J. Frigerio, A. Samarelli, K. Gallacher, E. Calandrini, G. Isella, D. J. Paul, M. Ortolani, and P. Biagioni, "Midinfrared plasmon-enhanced spectroscopy with germanium antennas on silicon substrates," Nano Lett. **15**, 7225–7231 (2015).
21. T. Hanke, G. Krauss, D. Träutlein, B. Wild, R. Bratschitsch, and A. Leitenstorfer, "Efficient nonlinear light emission of single gold optical antennas driven by few-cycle near-infrared pulses," Phys. Rev. Lett. **103**, 257404 (2009).
22. M. Kauranen and A. V. Zayats, "Nonlinear plasmonics," Nat. Photonics **6**, 737–748 (2012).
23. N. Pfullmann, C. Waltermann, M. Kovačev, V. Knittel, R. Bratschitsch, D. Akemeier, A. Hütten, A. Leitenstorfer, and U. Morgner, "Nano-antenna-assisted harmonic generation," Appl. Phys. B **113**, 75–79 (2013).
24. T. Rybka, M. Ludwig, M. F. Schmalz, V. Knittel, D. Brida, and A. Leitenstorfer, "Sub-cycle optical phase control of nanotunnelling in the single-electron regime," Nat. Photonics **10**, 667–670 (2016).
25. R. Soref, "Mid-infrared photonics in silicon and germanium," Nat. Photonics **4**, 495–497 (2010).
26. F. Scotognella, G. D. Valle, S. A. R. Kandada, M. Zavelani-Rossi, S. Longhi, G. Lanzani, and F. Tassone, "Plasmonics in heavily-doped semiconductor nanocrystals," Eur. Phys. J. B **86**, 154 (2013).
27. S. Law, L. Yu, A. Rosenberg, and D. Wasserman, "All-semiconductor plasmonic nanoantennas for infrared sensing," Nano Lett. **13**, 4569–4574 (2013).
28. F. B. Barho, F. Gonzalez-Posada, M.-J. Milla, M. Bomers, L. Cerutti, E. Tournié, and T. Taliercio, "Highly doped semiconductor plasmonic nanoantenna arrays for polarization selective broadband surface-enhanced infrared absorption spectroscopy of vanillin," Nanophotonics **7**, 507–516 (2018).
29. G. V. Naik, V. M. Shalaev, and A. Boltasseva, "Alternative plasmonic materials: beyond gold and silver," Adv. Mater. **25**, 3264–3294 (2013).
30. J. Frigerio, A. Ballabio, G. Isella, E. Sakat, G. Pellegrini, P. Biagioni, M. Bollani, E. Napolitani, C. Manganelli, M. Virgilio, A. Grupp, M. P. Fischer, D. Brida, K. Gallacher, D. J. Paul, L. Baldassarre, P. Calvani, V. Giliberti, A. Nucara, and M. Ortolani, "Tunability of the dielectric function of heavily doped germanium thin films for mid-infrared plasmonics," Phys. Rev. B **94**, 85202 (2016).
31. M. P. Fischer, A. Riede, K. Gallacher, J. Frigerio, G. Pellegrini, M. Ortolani, D. J. Paul, G. Isella, A. Leitenstorfer, P. Biagioni, and D. Brida, "Mid infrared nonlinear plasmonics using germanium nanoantennas on silicon substrates," Light Sci. Appl. **7**, 106 (2018).
32. N. Maccaferri, K. E. Gregorczyk, T. V. A. G. de Oliveira, M. Kataja, S. van Dijken, Z. Pirzadeh, A. Dmitriev, J. Åkerman, M. Knez, and P. Vavassori, "Ultrasensitive and label-free molecular-level detection enabled by light phase control in magnetoplasmonic nanoantennas," Nat. Commun. **6**, 6150 (2015).
33. R. Verre, N. Maccaferri, K. Fleischer, M. Svedendahl, N. O. Länk, A. Dmitriev, P. Vavassori, I. V. Shvets, and M. Käll, "Polarization conversion-based molecular sensing using anisotropic plasmonic metasurfaces," Nanoscale **8**, 10576–10581 (2016).
34. T. Hanke, J. Cesar, V. Knittel, A. Trügler, U. Hohenester, A. Leitenstorfer, and R. Bratschitsch, "Tailoring spatiotemporal light confinement in single plasmonic nanoantennas," Nano Lett. **12**, 992–996 (2012).
35. N. Accanto, L. Piatkowski, J. Renger, and N. F. van Hulst, "Capturing the optical phase response of nanoantennas by coherent second-harmonic microscopy," Nano Lett. **14**, 4078–4082 (2014).
36. E. Mårsell, A. Losquin, R. Svärd, M. Miranda, C. Guo, A. Harth, E. Lorek, J. Mauritsson, C. L. Arnold, H. Xu, A. L'Huillier, and A. Mikkelsen, "Nanoscale imaging of local few-femtosecond near-field dynamics within a single plasmonic nanoantenna," Nano Lett. **15**, 6601–6608 (2015).
37. F. Masia, W. Langbein, and P. Borri, "Measurement of the dynamics of plasmons inside individual gold nanoparticles using a femtosecond phase-resolved microscope," Phys. Rev. B **85**, 235403 (2012).
38. L. Piatkowski, N. Accanto, and N. F. van Hulst, "Ultrafast meets ultrasmall: controlling nanoantennas and molecules," ACS Photon. **3**, 1401–1414 (2016).
39. J. S. Huang, D. V. Voronine, P. Tuchscherer, T. Brixner, and B. Hecht, "Deterministic spatiotemporal control of optical fields in nanoantennas and plasmonic circuits," Phys. Rev. B **79**, 195441 (2009).
40. R. Faggiani, A. Losquin, J. Yang, E. Mårsell, A. Mikkelsen, and P. Lalanne, "Modal analysis of the ultrafast dynamics of optical nanoresonators," ACS Photon. **4**, 897–904 (2017).
41. B. Metzger, M. Hentschel, M. Lippitz, and H. Giessen, "Third-harmonic spectroscopy and modeling of the nonlinear response of plasmonic nanoantennas," Opt. Lett. **37**, 4741–4743 (2012).
42. Q. Sun, K. Ueno, H. Yu, A. Kubo, Y. Matsuo, and H. Misawa, "Direct imaging of the near field and dynamics of surface plasmon resonance on gold nanostructures using photoemission electron microscopy," Light Sci. Appl. **2**, e118 (2013).

43. A. Anderson, K. S. Deryckx, X. G. Xu, G. Steinmeyer, and M. B. Raschke, "Few-femtosecond plasmon dephasing of a single metallic nanostructure from optical response function reconstruction by interferometric frequency resolved optical gating," Nano Lett. **10**, 2519–2524 (2010).
44. P. D. Keathley, W. P. Putnam, P. Vasireddy, R. G. Hobbs, Y. Yang, K. K. Berggren, and F. X. Kärtner, "Vanishing carrier-envelope-phase-sensitive response in optical-field photoemission from plasmonic nanoantennas," Nat. Phys. **15**, 1128–1133 (2019).
45. M. Savoini, S. Grübel, S. Bagiante, H. Sigg, T. Feurer, P. Beaud, and S. L. Johnson, "THz near-field enhancement by means of isolated dipolar antennas: the effect of finite sample size," Opt. Express **24**, 4552–4562 (2016).
46. M. Shalaby, H. Merbold, M. Peccianti, L. Razzari, G. Sharma, T. Ozaki, R. Morandotti, T. Feurer, A. Weber, L. Heyderman, B. Patterson, and H. Sigg, "Concurrent field enhancement and high transmission of THz radiation in nanoslit arrays," Appl. Phys. Lett. **99**, 041110 (2011).
47. P. Peier, H. Merbold, V. Pahinin, K. A. Nelson, and T. Feurer, "Imaging of THz waves in 2D photonic crystal structures embedded in a slab waveguide," New J. Phys. **12**, 013014 (2010).
48. M. Walther and A. Bitzer, "Electromagnetic wave propagation close to microstructures studied by time and phase-resolved THz near-field imaging," J. Infrared Millim. Terahertz Waves **32**, 1020–1030 (2010).
49. O. Buchnev, J. Wallauer, M. Walther, M. Kaczmarek, N. I. Zheludev, and V. A. Fedotov, "Controlling intensity and phase of terahertz radiation with an optically thin liquid crystal-loaded metamaterial," Appl. Phys. Lett. **103**, 141904 (2013).
50. I.-C. Benea-Chelmus, Y. Salamin, F. F. Settembrini, Y. Fedoryshyn, W. Heni, D. L. Elder, L. R. Dalton, J. Leuthold, and J. Faist, "Electro-optic interface for ultrasensitive intracavity electric field measurements at microwave and terahertz frequencies," Optica **7**, 498–505 (2020).
51. J. Wallauer and M. Walther, "Fano line shape and phase reversal in a split-ring resonator based metamaterial," Phys. Rev. B **88**, 195118 (2013).
52. C. A. Schmuttenmaer, "Exploring dynamics in the far-infrared with terahertz spectroscopy," Chem. Rev. **104**, 1759–1780 (2004).
53. H.-K. Nienhuys and V. Sundström, "Intrinsic complications in the analysis of optical-pump, terahertz probe experiments," Phys. Rev. B **71**, 235110 (2005).
54. M. Tonouchi, "Cutting-edge terahertz technology," Nat. Photonics **1**, 97–105 (2007).
55. M. A. Alonso, "Wigner functions in optics: describing beams as ray bundles and pulses as particle ensembles," Adv. Opt. Photon. **3**, 272–365 (2011).
56. S. Keiber, S. Sederberg, A. Schwarz, M. Trubetskov, V. Pervak, F. Krausz, and N. Karpowicz, "Electro-optic sampling of near-infrared waveforms," Nat. Photonics **10**, 159–162 (2016).
57. J. Shan, A. S. Weling, E. Knoesel, L. Bartels, M. Bonn, A. Nahata, G. A. Reider, and T. F. Heinz, "Single-shot measurement of terahertz electromagnetic pulses by use of electro-optic sampling," Opt. Lett. **25**, 426–428 (2000).
58. B. Steffen, C. Gerth, M. Caselle, M. Felber, T. Kozak, D. R. Makowski, U. Mavrič, A. Mielczarek, P. Peier, K. Przygoda, and L. Rota, "Compact single-shot electro-optic detection system for THz pulses with femtosecond time resolution at MHz repetition rates," Rev. Sci. Instrum. **91**, 045123 (2020).
59. M. M. Mirza, H. Zhou, P. Velha, X. Li, K. E. Docherty, A. Samarelli, G. Ternent, and D. J. Paul, "Nanofabrication of high aspect ratio (∼50:1) sub-10 nm silicon nanowires using inductively coupled plasma etching," J. Vac. Sci. Technol. B **30**, 06FF02 (2012).
60. F. Junginger, A. Sell, O. Schubert, B. Mayer, D. Brida, M. Marangoni, G. Cerullo, A. Leitenstorfer, and R. Huber, "Single-cycle multiterahertz transients with peak fields above 10 MV/cm," Opt. Lett. **35**, 2645–2647 (2010).
61. A. Grupp, A. Budweg, M. P. Fischer, J. Allerbeck, G. Soavi, A. Leitenstorfer, and D. Brida, "Broadly tunable ultrafast pump-probe system operating at multi-kHz repetition rate," J. Opt. **20**, 014005 (2018).
62. M. Bradler, P. Baum, and E. Riedle, "Femtosecond continuum generation in bulk laser host materials with sub-μJ pump pulses," Appl. Phys. B **97**, 561–574 (2009).
63. Lumerical Solutions, Inc., FDTD, Version 8.17.1157 (2013).